Supplementary Material for: Coherence of a non-equilibrium polariton condensate across the interaction-mediated phase transition

P. Comaron,[1,*] E. Estrecho,[2,†] M. Wurdack,[2,‡] M. Pieczarka,[2,3] M. Steger,[4,§] D. W. Snoke,[4] K. West,[5] L. N. Pfeiffer,[5] A. G. Truscott,[6] M. Matuszewski,[7,8] M. Szymanska,[1,¶] and E. A. Ostrovskaya[2,**]

[1]*Department of Physics and Astronomy, University College London, Gower Street, London, WC1E 6BT, United Kingdom*

[2]*ARC Centre of Excellence in Future Low-Energy Electronics Technologies and Department of Quantum Science and Technology, Research School of Physics, The Australian National University, Canberra, ACT 2601, Australia*

[3]*Department of Experimental Physics, Faculty of Fundamental Problems of Technology, Wroclaw University of Science and Technology, Wyb. Wyspiańskiego 27, 50-370 Wrocław Poland*

[4]*Department of Physics and Astronomy, University of Pittsburgh, Pittsburgh, PA 15260, USA*

[5]*Department of Electrical Engineering, Princeton University, Princeton, NJ 08544, USA*

[6]*Department of Quantum Science and Technology, Research School of Physics, The Australian National University, Canberra, ACT 2601, Australia*

[7]*Institute of Physics, Polish Academy of Sciences, Al. Lotnikow 32/46, 02-668 Warsaw, Poland*

[8]*Center for Theoretical Physics, Polish Academy of Sciences, Al. Lotnikow 32/46, 02-668 Warsaw, Poland*

(Dated: January 24, 2025)

Supplementary Note 1: Berezinskii-Kosterlitz-Thouless transition and its properties in nonequilibrium systems

The Berezinskii-Kosterlitz-Thouless (BKT) phase transition is a topological transition that occurs in two-dimensional systems, driven by the behavior of vortex-antivortex pairs rather than conventional symmetry breaking. At low temperatures, these pairs are bound, leading to quasi-long-range order where spatial correlations decay algebraically. As the temperature rises and crosses a critical threshold, thermal fluctuations cause the pairs to dissociate into free vortices, resulting in a transition to a disordered phase with exponential decay of correlations.

A comparison between experimental and numerical studies of the Berezinskii-Kosterlitz-Thouless (BKT) transition in driven-dissipative systems and its traditional equilibrium counterpart reveals that the fundamental processes—vortex-antivortex pairing and coherence decay—are essentially the same [1, 2]. As the control parameter increases (in the case of polaritons, the increasing laser power strength act as the control parameter, substituting the decreasing temperature), both systems undergo a phase transition: from a disordered phase where free vortices proliferate and correlations decay exponentially, to a quasi-ordered phase where vortices form bound pairs and spatial correlations follow an algebraic decay.

Due to technical difficulties, directly observing the spontaneous pairing and dissociation of the vortices, which serves as a definitive marker of the BKT transition, remains a significant challenge in polariton systems. Most experimental methods rely on time-averaging or multiple realizations of the condensate, which tend to obscure the ultrafast and stochastic vortex dynamics. Single-shot, time-resolved imaging techniques have been proposed to address this issue [3], but these are technically demanding. Due to these challenges, first-order spatial coherence has become the preferred observable for probing the phase transition in polariton systems, readily obtainable from the light escaping the optical cavity. Experiments have shown that polaritons undergo a transition from exponential to power-law decay of spatial coherence [1, 2, 4, 5].

In the equilibrium BKT case, the power-law decay exponent α, which characterizes the quasi-ordered state, is theoretically constrained by energetic considerations to a maximum value of $\alpha = 0.25$. In polariton systems, this upper bound also holds in the so-called "equilibrium" limit of the non-conservative system [4, 5], while, outside this limit, the phase transition behaves differently, with the exponent α exceeding 0.25 due to the absence of the same energetic constraints [2].

Supplementary Note 2: Other experimental details

Polariton density - We performed direct density measurements following a procedure similar to the one used in Ref. [6]. We measured the output power P_{out} of the condensate emanating from a small region of interest with area A created by a real-space filter. For each sample detuning (or sample position), the polariton lifetime τ_{pol} is

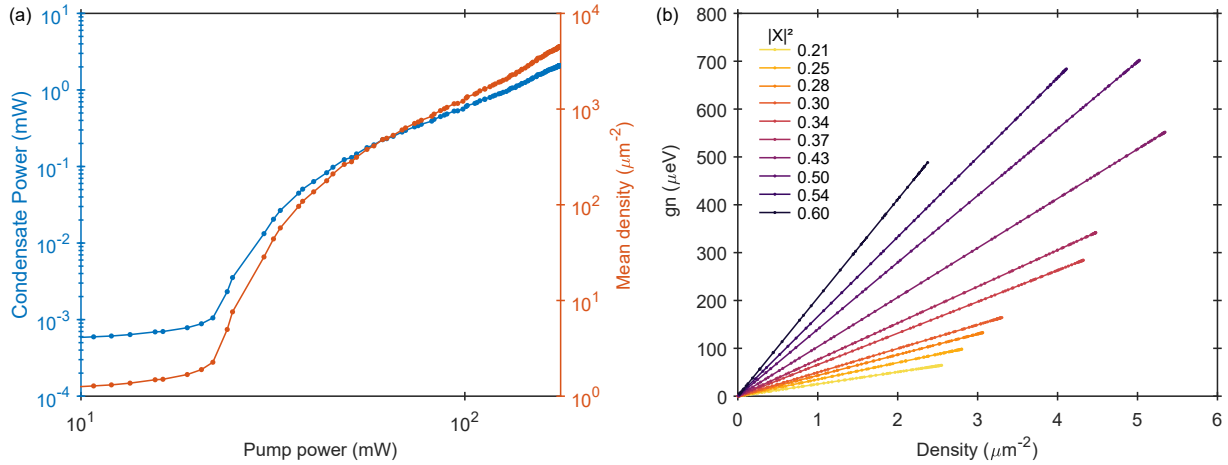

Figure S1: **Experimental densities and interaction energies.** **a**, Condensate power and mean density as a function of pump power corresponding to the data set in Fig. 2 of the main text. **b**, Range of interaction energies and densities probed for all excitonic fractions $|X|^2$ explored in this work.

calculated from the excitonic fraction $|X|^2$, resulting in the following conversion to polariton density:

$$n = \frac{\tau_{pol}}{h\nu\eta A} P_{out}$$

where $h\nu$ is the polariton energy, and η is the collection efficiency. We previously calibrated η at the power measurement position using a 775-nm laser reflected by a mirror at the sample position. We have also taken into account the reflectivity ratio between the top and bottom DBRs of the sample (~80%) in the collection efficiency [6] Fig. S1a shows the plot of the dependence of density on the pump power corresponding to the dataset in Fig. 2 of the main text. It also shows the input-output curve. The threshold density is $\approx 2\mu\text{m}^{-2}$.

Interaction energy - The interaction energy is extracted from the measured polariton density using the formula $E_{int} = gn$, where g is the polariton-polaritton interaction strength defined as $g = |X|^4 g_X/(2N_{qw})$ [6], where $g_X = 13.5\ \mu\text{eV}\cdot\mu\text{m}^{-2}$ [7] is the exciton-exciton interaction strength, and $N_{qw} = 12$ is the number of quantum wells in our sample. In this work, gn is increased by either increasing the density or the excitonic fraction $|X|^2$. We do not use the condensate blueshift to extract the interaction strength as it also includes the interaction with the reservoir [7]. The range of polariton densities and interaction energies probed in this work are presented in Fig. S1.

Healing length - The healing length ξ of the condensate is calculated from the measured density n using the formula $\xi = \frac{\hbar}{\sqrt{2mgn}}$, where $\hbar$ is Planck's constant, m is the polariton effective mass, and g is the polariton-polariton interaction strength. The mass m is extracted from the polariton dispersion at each detuning.

Supplementary Note 3: Additional information on numerical simulations and analysis

Steady-state calculations.- We solve the stochastic equations, Eq. (2) of the main text, starting from a random noise configuration resembling a disordered phase, and letting evolve the system until a non-equilibrium steady state (NESS) is reached. In our model both initial noise and the noise during the time evolution simulate quantum fluctuations, where the Wiener noise in the system is introduced self-consistently in the model. In order to simulate the experimental measurements, the polariton dynamics is left to evolve for a long time (from a minimum of 5ns to a maximum of 100ns, depending on the equilibration times) in order to allow the system to reach a full NESS configuration. In Fig. S2 we plot the typical results of a single simulation at a given $|X|^2$ and pump strength P_0. The static pumping profile is shown in panel **a**, while the steady-state density and phase of the polaritons are depicted in panels **b** and **d**, respectively. The total polariton density $\langle|\psi|^2\rangle_{(x,y)}$ averaged over real-space is plotted in panel **c**.

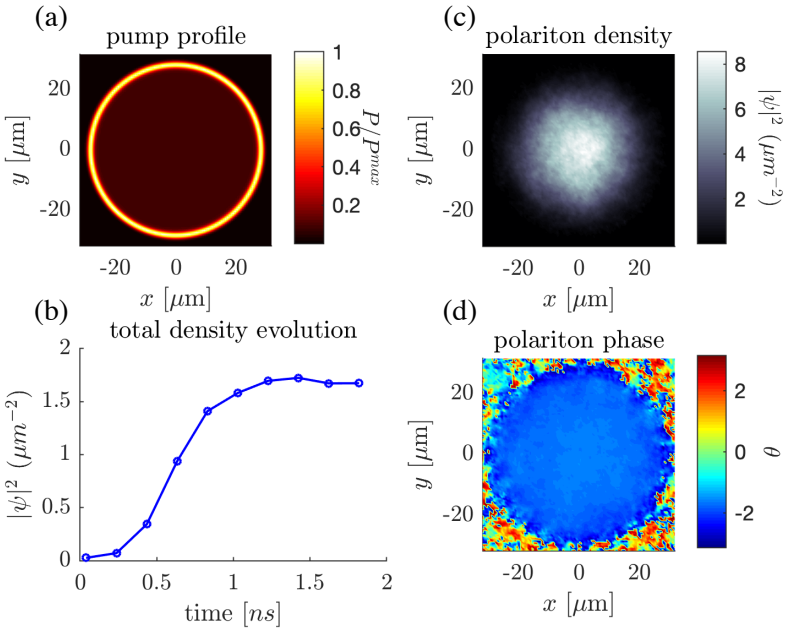

Figure S2: **Numerical simulations**. **a**, The ring-shaped pump profile $P(\mathbf{r})$ with $P_0 = 0.04$. **b**, The temporal evolution of the total density of polaritons up to 2 ns, towards the steady state, for an excitonic fraction of $|X|^2 = 0.34$. The image of **c** the real-space denisty distribution and **d** phase of the polaritons at $t = 2$ns.

Polariton coherence.- Once the NESS is reached for a set of $\mathcal{N} = 100$ stochastic realisations (each starting from a different noise configuration) we calculate the spatial first-order correlation function as described in the "Modelling of the polariton field" paragraph of the Methods section of the main paper. In order to obtain a smooth NESS correlator, we integrate over different snapshots of the steady-state, as well as over the $\mathcal{N}$ realizations. In Fig. S3 we show in panel **a** a carpet plot of the spatial correlator evolution in time. After an initial growth, the system reaches a NESS. In the panels **b** we report the time-averaged polariton density $\langle n(r)\rangle_t \equiv \left\langle |\psi(t)|^2 \right\rangle_{\mathcal{N},t}$ (black curve) as well as the single-time and time-averaged correlators (blue and red solid curves, respectively). In panel **c** we repropose the same curves as in **b** but in log-log scale.

Procedure for fitting the spatial coherence

Details on the curve fitting.- As explained in the main text, at the section "Density dependence of coherence at a fixed excitonic fraction", to extract the relevant decay exponents, we fit the steady-state spatial correlation functions, of both the experimental and numerical data, to both a power-law and an exponential curve. In a uniform system, the comparison between the RMS deviations of the exponential and power-law fitting curves to a particular steady-state correlator allow to identify whether that particular state is better described by an algebraic or exponential decay.

Following Refs. [5, 8], as a measure of the quality of the fitting procedure, we calculate the root mean square (RMS) deviation of the fit, defined as

$$\mathrm{RMS} = \sum_i \frac{(g^{(1)}(r_i) - g^{(1)}_{\mathrm{fit}}(r_i))^2}{(g^{(1)}(r_i))^2}; \tag{S1}$$

here the index i identify the position in real-space. In Fig. S4 we display the RMS distributions as a function of the system density, along the excitonic-fraction crossover. We note that, at low densities, independently from the excitonic fraction, the spatial correlator is always better described by an exponential decay, since the blue RMS is always lower than the red RMS. Only for excitonic fractions $|X|^2$ around 0.4, for densities around $2 \times 10^{-3} \mu\mathrm{m}^{-2}$, the two RMS becomes comparable. This suggests that the finite size effects introduced by the strong excitonic-reservoir confinement always have a strong effect.

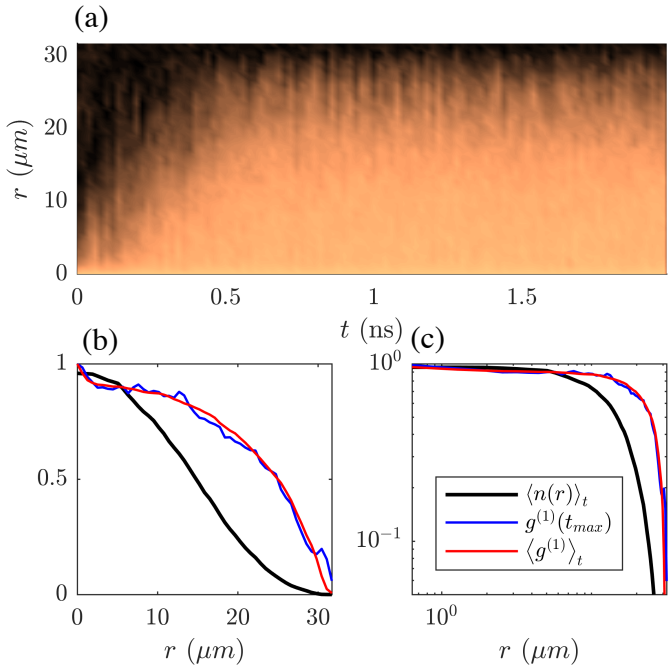

Figure S3: **Numerical coherence**. **a**, The first order correlation function is plotted as a function of time along the evolution of the polaritons towards the steady state, for the case depicted in Fig. S2. The time-integrated density and time-integrated spatial correlations, together with the first-order correlation function calculated at the end of the time-integration window, are plotted in panels **b** and **c** in linear-linear and log-log scales, respectively. The time-integration is applied in the window $2 < t < 4$ ns.

Details on the extraction of the momentum occupation

Momentum occupation.- In this section, we review the procedure we use to measure and calculate the momentum occupation $\mathcal{N}(k)$. The momentum distribution is proportional to the CCD intensity $I_{\rm CCD}$, namely $\mathcal{N}(k) = \mathcal{A} \times I_{\rm CCD}$. To find $\mathcal{A}$, we can assume the actual momentum distribution to be $n_k(\mathbf{k}) = QI_{\rm CCD}$, where Q is some scaling determined from the recorded power. The relation to experiments is

$$\frac{dN_{ph}}{dt}\frac{1}{\eta} = \int QI_{\rm CCD}(k)\tau(k)d^2k \tag{S2}$$

where we assume the distribution to be cylindrically symmetric. The polariton lifetime $\tau(k) = \tau(|X|^2)$ can be calculated from the excitonic fraction, which is function of k. However, we do not expect a strong role and we therfore approximate the polariton lifetime as $\tau(k) = \tau_0$. Then, the occupation $\mathcal{N}$ can be calculated from the density of states $N(k)$ as $\mathcal{N} = n_k(k)/N(k)$. Following the reasoning in [9], the density of states can be calculated assuming a flat distribution and negligible interaction:

$$N(k) = \Gamma\frac{A_{trap}}{(2\pi)^2}kdkd\phi = \Gamma\frac{A_{trap}}{2\pi}kdk, \tag{S3}$$

which correspond to Eq. (A6) of Ref. [9], where $\Gamma = 2$ stands for the polariton state spin degeneracy. Eq. S2 can be rewritten as

$$\frac{dN_{ph}}{dt}\frac{\tau_0}{\eta} = N_{pol} = A_f\langle n\rangle = \int 2\pi QI_{\rm CCD}(k)kd^2k. \tag{S4}$$

The occupation finally reads:

$$\mathcal{N}(\mathbf{k}) = \frac{A_f(|X|^2)\langle n\rangle}{\int 2\pi I_{\rm CCD}(\mathbf{k})kdk}\frac{I_{\rm CCD}(\mathbf{k})}{\Gamma A_{trap}(2\pi)^{-1}kdk} = \mathcal{A} \times I_{\rm CCD}(\mathbf{k}). \tag{S5}$$

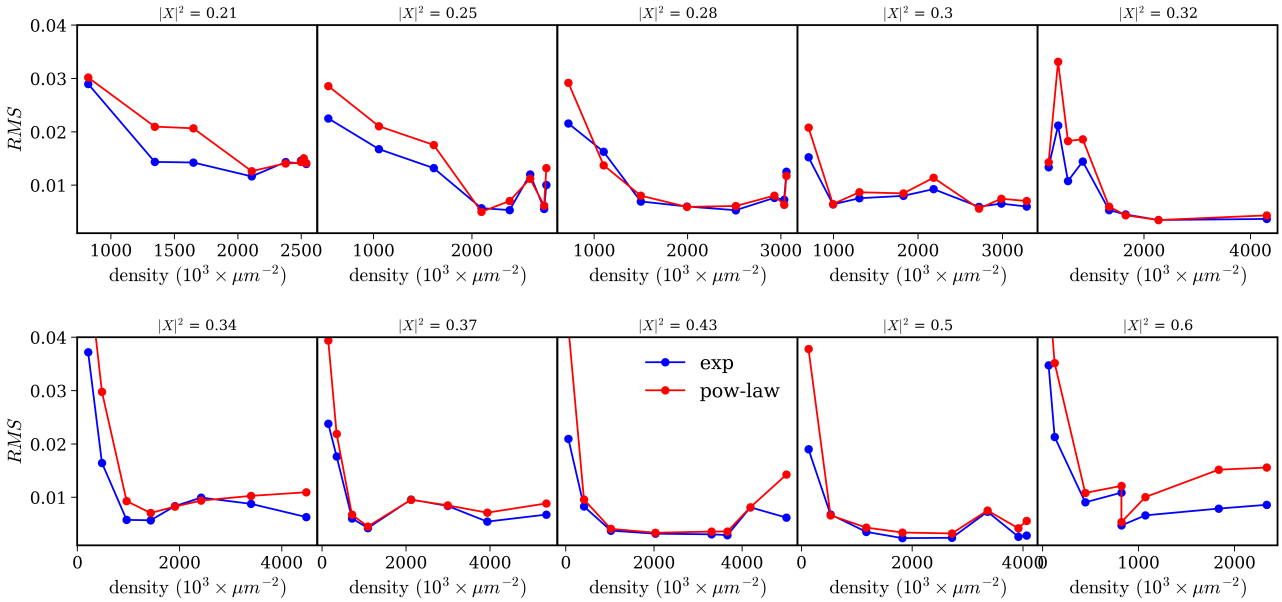

Figure S4: **Residuals of the fits**. The root mean square (RMS) of the fit to the exponential (blue) and power-law (red) curves to the experimental data are reported here for different densities and excitonic fractions $|X|^2$.

* These two authors contributed equally to this work; p.comaron@ucl.ac.uk
† These two authors contributed equally to this work; eliezer.estrecho@anu.edu.au
‡ current address: Hansen Experimental Physics Laboratory and Department of Neurosurgery, Stanford University, Stanford, CA 94305
§ current address: National Renewable Energy Laboratory, Golden, CO 80401, USA
¶ m.szymanska@ucl.ac.uk
** elena.ostrovskaya@anu.edu.au

Supplementary References

[1] W. Nitsche *et al.*, Algebraic order and the berezinskii-kosterlitz-thouless transition in an exciton-polariton gas, Phys. Rev. B **90**, 205430 (2014).

[2] G. Dagvadorj, J. M. Fellows, S. Matyjaśkiewicz, F. M. Marchetti, I. Carusotto, and M. H. Szymańska, Nonequilibrium phase transition in a two-dimensional driven open quantum system, Phys. Rev. X **5**, 041028 (2015).

[3] E. Estrecho, T. Gao, N. Bobrovska, M. D. Fraser, M. Steger, L. Pfeiffer, K. West, T. C. H. Liew, M. Matuszewski, D. W. Snoke, A. G. Truscott, and E. A. Ostrovskaya, Single-shot condensation of exciton polaritons and the hole burning effect, Nature Communications **9**, 2944 (2018).

[4] D. Caputo, D. Ballarini, G. Dagvadorj, C. Sánchez Muñoz, M. De Giorgi, L. Dominici, K. West, L. N. Pfeiffer, G. Gigli, F. P. Laussy, M. H. Szymańska, and D. Sanvitto, Topological order and thermal equilibrium in polariton condensates, Nature Materials **17**, 145 (2018).

[5] P. Comaron, I. Carusotto, M. H. Szymańska, and N. P. Proukakis, Non-equilibrium berezinskii-kosterlitz-thouless transition in driven-dissipative condensates, Europhysics Letters **133**, 17002 (2021).

[6] E. Estrecho, T. Gao, N. Bobrovska, D. Comber-Todd, M. D. Fraser, M. Steger, K. West, L. N. Pfeiffer, J. Levinsen, M. M. Parish, T. C. H. Liew, M. Matuszewski, D. W. Snoke, A. G. Truscott, and E. A. Ostrovskaya, Direct measurement of polariton-polariton interaction strength in the thomas-fermi regime of exciton-polariton condensation, Phys. Rev. B **100**, 035306 (2019).

[7] M. Pieczarka, E. Estrecho, M. Boozarjmehr, O. Bleu, M. Steger, K. West, L. N. Pfeiffer, D. W. Snoke, J. Levinsen, M. M. Parish, A. G. Truscott, and E. A. Ostrovskaya, Observation of quantum depletion in a non-equilibrium exciton–polariton condensate, Nature Communications **11**, 429 (2020).

[8] D. Caputo, D. Ballarini, G. Dagvadorj, C. Sánchez Muñoz, M. De Giorgi, L. Dominici, K. West, L. N. Pfeiffer, G. Gigli, F. P. Laussy, M. H. Szymańska, and D. Sanvitto, Topological order and thermal equilibrium in polariton condensates, Nature Materials **17**, 145 EP (2017).

[9] M. Pieczarka, M. Boozarjmehr, E. Estrecho, Y. Yoon, M. Steger, K. West, L. N. Pfeiffer, K. A. Nelson, D. W. Snoke, A. G. Truscott, and E. A. Ostrovskaya, Effect of optically induced potential on the energy of trapped exciton polaritons below

the condensation threshold, Phys. Rev. B **100**, 085301 (2019).